Spin-Orbital Superstructure in Strained Ferrimagnetic Perovskite Cobalt Oxide

J. Fujioka,[1] Y. Yamasaki,[2] H. Nakao,[2] R. Kumai,[2] Y. Murakami,[2] M. Nakamura,[3] M. Kawasaki,[1,3] and Y. Tokura[1,3]

[1]*Department of Applied Physics and Quantum-Phase Electronics Center (QPEC), University of Tokyo, Hongo, Tokyo 113-8656, Japan*
[2]*Condensed Matter Research Center (CMRC) and Photon Factory, Institute of Materials Structure Science (IMSS), High Energy Accelerator Research Organization (KEK), Tsukuba 305-0801, Japan*
[3]*RIKEN Center for Emergent Matter Science (CEMS), Wako 351-0198, Japan*

(Received 1 March 2013; published 9 July 2013)

We have investigated the Co-3*d* spin-orbital state in a thin film of perovskite $LaCoO_3$ to clarify the origin of strain induced spontaneous magnetization ($T_C = 94$ K) by means of x-ray diffraction, optical spectroscopy, and magnetization measurements. A lattice distortion with the propagation vector $(1/4\ -1/4\ 1/4)$ and an anomalous activation of optical phonons coupled to Co-3*d* orbital are observed below 126 K. Combined with the azimuthal angle analysis of superlattice reflection, we propose that the ordering of Co-3*d* orbital promoted by an epitaxial strain produces a unique ferrimagnetic structure.

DOI: 10.1103/PhysRevLett.111.027206 PACS numbers: 75.25.Dk, 75.70.−i, 78.30.−j, 78.70.Ck

The interplay among charge, spin, and orbital degrees of freedom in strongly correlated electron systems provides a unique arena in which to produce emergent quantum states such as charge-orbital ordering, magnetically induced ferroelectrics (multiferroelectricity), and unconventional superconductivity. The critical control of competing phases in the *d*-electron transition-metal oxides can be achieved by small perturbations on the material tuning parameter such as the effective one-electron bandwidth and band filling. For example, in perovskite manganites, a tiny change in the lattice distortion or nominal *d*-electron concentration via the chemical doping gives rise to the phase switching between the charge-orbital ordered state and the ferromagnetic metallic one, leading to a dramatic change in the charge transport, magnetic, and optical properties [1].

Aside from these conventional approaches, in a certain class of transition-metal compounds there is a unique material tuning parameter, that is, the spin-state variability (low-, intermediate-, and high-spin states) of the constituent magnetic ions. One such example is the perovskite $LaCoO_3$, which is known as a prototype of the spin-state crossover material and has received much attention for these decades [2–10]. In this system, the nominally trivalent Co ion (Co^{3+}) forms the three-dimensional network with corner-sharing CoO_6 octahedra, and may take three different spin states: the low-spin (LS) state with filled $3d\ t_{2g}$ manifold ($S = 0$), intermediate-spin (IS) state with active e_g and t_{2g} orbital degrees of freedom ($S = 1$), and high-spin (HS) state with active t_{2g} orbital degree of freedom ($S = 2$), as shown in Fig. 1(a). Indeed, $LaCoO_3$ exhibits a thermally induced crossover from nonmagnetic to paramagnetic around 90 K [Fig. 1(b)] attributed to the spin state change from the LS state to the IS or HS state [2,3]. It has also been recognized that the spin state is amenable to various external stimuli. A spectacular example is the strain induced IS and/or HS state and spontaneous magnetization; the nonmagnetic insulating phase in the bulk crystal is turned into the magnetic one with spontaneous magnetization in the epitaxial thin film of $LaCoO_3$ while keeping its insulating nature [11–14]. This is quite unique since many other stimuli such as the chemical substitution [6] [Fig. 1(b)] and external pressure [15] rather stabilize the LS state in the bulk form except the case under an extremely high magnetic field [16].

Several models have recently been proposed to explain the strain induced magnetization: the chemically inhomogeneous state including ferromagnetic metallic patches originating from unintentionally doped carriers, the ferromagnetism mediated by the orbital ordering, and the unique ferrimagnetism or ferromagnetism due to the spin state disproportionation [11–14,17–19]. However, to the best of our knowledge, there is no experimental report exploring the microscopic spin-orbital structure for this enigmatic magnetic phase, which is indispensable to unveil the mechanism of strain induced magnetization. Here using a high-quality epitaxial thin film of $LaCoO_3$, we show that the unique orbital ordering of Co ions composed of the IS and/or HS state gives rise to the ferrimagnetic structure, suggesting the key role of competing exchange interactions due to the strong spin-orbital entanglement inherent to the strain induced magnetic spin state of Co ions.

The single crystalline film (60 nm thick) of $LaCoO_3$ is fabricated on the $(LaAlO_3)_{0.3}(SrAl_{0.5}Ta_{0.5}O_3)_{0.7}$ (LSAT) substrate with (110) orientation by pulsed laser deposition. Measurements of magnetization were performed by using a SQUID magnetometer. The spectra of dielectric constant were acquired by the reflectivity spectra on the basis of Kramers-Kronig analysis, which were measured by a Fourier transform spectrometer (grating-type monochromator) in the photon energy region of 0.008–0.7 eV (0.5–5 eV). The synchrotron-radiation x-ray diffraction was performed to detect the fundamental and superlattice reflection at BL-3A and BL-4C, Photon Factory of KEK, Japan.

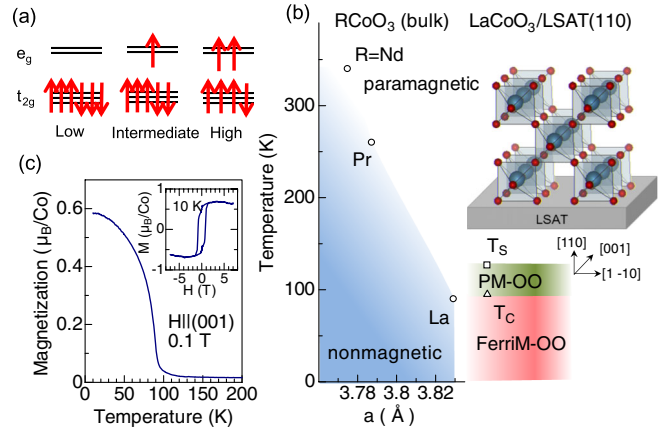

FIG. 1 (color online). (a) Schematic view of the spin states of trivalent Co ion (Co^{3+}); the low spin-, intermediate spin-, and high spin states. The arrows denote the electron spins. (b) Electronic phase diagrams of the tensile strained $LaCoO_3$ and the bulk $RCoO_3$ (R is rare earth element). The circle indicates the typical spin state crossover temperature from nonmagnetic to paramagnetic state as determined by the linear thermal expansion [6]. The square and triangle denote the transition temperature of orbital ordering (OO) and that of the ferrimagnetic (FerriM) ordering, respectively. The inset shows the schematic view of the tensile strained $LaCoO_3$ film grown on LSAT(110) substrate. The lattice constant (a) is defined as the cubic root of the unit cell volume in the pseudocubic setting. (c) Temperature dependence of in-plane magnetization. The inset shows the in-plane magnetization (M) curve at 10 K.

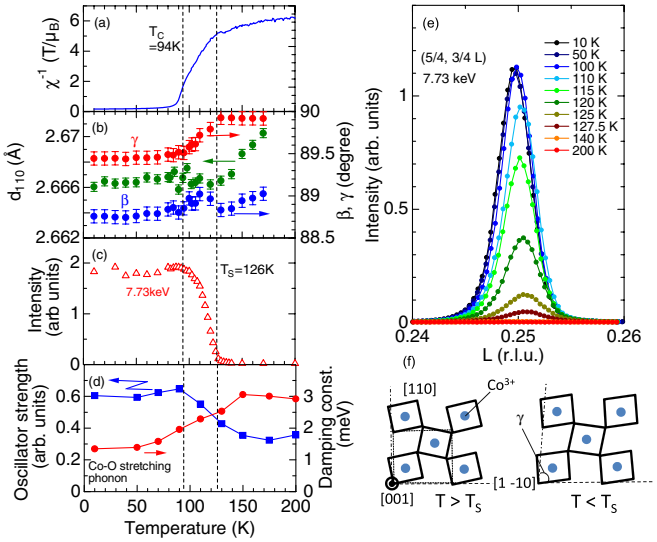

FIG. 2 (color online). Temperature dependence of (a) inverse susceptibility (χ^{-1}), (b) d_{110} (green), β (blue), and γ (red), (c) integrated intensity of superlattice reflection measured at 7.73 keV, (d) oscillator strength (square) and damping constant (circle) of the Co-O stretching optical phonon. (e) Profiles of superlattice reflection at (5/4, 3/4, 1/4). Here the reciprocal lattice units are represented in the basis of the LSAT substrate. r.l.u. means the reciprocal lattice unit. (f) Schematic view of the lattice distortion projected on the (001) plane. The dotted line indicates the unit cell of monoclinic phase with $I2/a$ symmetry (see Supplemental Material [20]).

Figure 1(c) shows the temperature dependence of the magnetization for the epitaxial thin film of $LaCoO_3$. The magnetic transition is observed as an onset of the magnetization at 94 K ($= T_C$), and the saturated moment at 10 K is about $0.7 \pm 0.1 \mu_B$/Co, which is comparable to that for the prevailing films on LSAT(001) substrate [11–14]. Figure 2(a) shows the temperature dependence of inverse magnetic susceptibility (χ^{-1}). The χ^{-1}-T curve shows a kink at 126 K as well as around T_C, suggesting the change in the magnetic exchange interaction around 126 K.

To clarify the anomaly of the magnetic susceptibility from the viewpoint of the crystal structure, we performed the x-ray diffraction experiment. We have pursued temperature dependence of several fundamental reflections at (110), (111), (311), and (321), and have calculated the lattice parameters of $LaCoO_3$: the out-of-plane lattice constant (d_{110}), the angle between [110] axis and [1 −10] one (γ) and that between [110] and [001] axes (β). We note that the in-plane lattice constants ([001] and [1 −10]) and the angle between them are locked to the substrate, while d_{110}, β, and γ may vary (see Supplemental Material [20]). Figure 2(b) shows the temperature dependence of d_{110}, β, and γ. With lowering temperature, d_{110} steeply decreases down to 126 K and undergoes minimal temperature dependence below 126 K. It is also clear that γ starts to deviate from 90° below 126 K. Moreover, we have identified a superlattice reflection characterized by the propagation vector $\mathbf{q} = (1/4\ -1/4\ 1/4)$ below 126 K. Figure 2(e) exemplifies the profile of superlattice reflection at (5/4 3/4 1/4). The intensity gradually increases below 126 K and nearly saturates below T_C [Fig. 2(c)]. These results point to the existence of the structural phase transition at 126 K ($= T_S$), which quadruples the unit cell of pseudocubic setting along the [100], [010], and [001] axes concomitantly with the shear-type lattice distortion along the [1 −10] direction as exemplified in Fig. 2(f).

The inset to Fig. 3(a) shows the scattering spectrum of (5/4 3/4 1/4) superlattice reflection as well as the absorption spectrum around Co K edge ($1s$-$4p$ intra-atomic transition) measured at 10 K. The scattered x ray includes both σ' and π' polarization components, while the incident x ray is nearly σ polarized. Here, σ and π denote the polarization component perpendicular and parallel to the scattering plane, respectively. The scattering spectrum exhibits a clear resonance with the Co K edge around 7.73 keV. We have analyzed the polarization of scattered x ray and azimuthal angle (ψ) dependence of the scattering intensity. Here ψ is defined as zero, when the x-ray polarization is approximately parallel to the [−3/4 5/4 0] direction. Figure 3(b) shows the scattering spectra in $\sigma \rightarrow \pi'$ geometry at various ψ. To cancel out the geometrical change of the scattering cross section in sweeping ψ, the spectra are normalized by the scattering intensity at

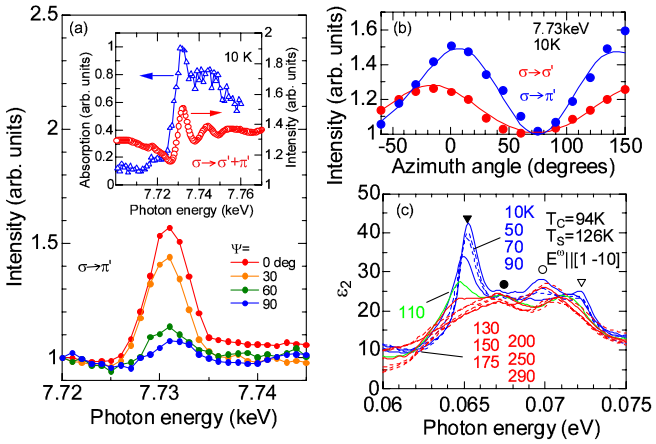

FIG. 3 (color online). (a) Energy spectra of the scattered intensity in $\sigma \rightarrow \pi'$ geometry. Inset is the energy spectra of the intensity of (5/4 3/4 1/4) diffraction (without polarization analysis, circles) in comparison with the x-ray absorption spectra (XAS) at Co K edge measured in the fluorescence yield method (triangles). (b) Azimuthal angle dependence of the resonant scattering intensity measured at 10 K ($< T_S$). The solid lines are the results of simulation of scattering intensity. (c) Energy spectra of imaginary part of the dielectric constant (ϵ_2) around 0.067 eV. The peak structures marked by closed triangle, closed circle, open circle, and open triangle are assigned to the Co-O stretching mode at 0.065, 0.067, 0.070, and 0.072 eV, respectively.

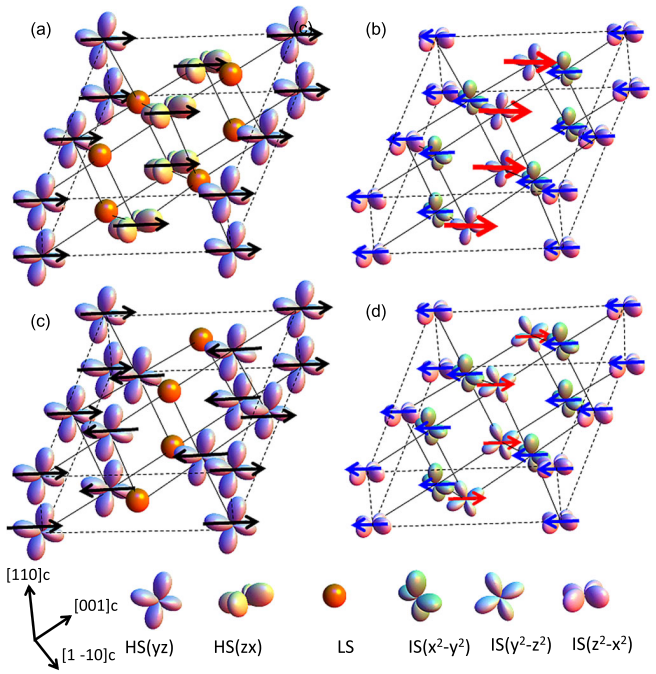

FIG. 4 (color online). The proposed models of the spin and orbital ordered structure: (a) High spin (HS)/low spin (LS)-state ordered state with the rocksalt type configuration. (b) Intermediate spin (IS)/HS-state ordered state. (c) HS/LS-state ordered state with 3/1 ratio. (d) homogeneous IS state. The lobes denote the e_g orbital of IS state and the active t_{2g} orbital of HS state. The t_{2g} orbital of IS state as well as the fully occupied, Hund's-rule coupled t_{2g} orbital is omitted for clarity. The dashed line indicates the unit cell of this spin-orbital superstructure.

7.72 keV, which is governed by the nonresonant signal. Remarkably, even in $\sigma \rightarrow \pi'$ geometry, the resonant structure is discernible and shows an appreciable ψ dependence. The normalized intensity clearly shows a periodic change as a function of ψ as shown in Fig. 3(b). A similar periodic feature is observed in $\sigma \rightarrow \sigma'$ geometry. This indicates that the resonant scattering at the Co K edge originates from the anisotropy of the tensor of susceptibility [21]. In other words, the local electronic and/or structural symmetry around the Co^{3+} ion is expected to be not cubic but anisotropic.

Further insight into the change of the crystal structure can be acquired by measurements of optical phonons. Figure 3(c) shows energy spectra of the imaginary part of the dielectric constant (ϵ_2). At room temperature, one can see two phonon modes at 0.067 and 0.070 eV, while an additional two peaks grow in intensity around 0.065 and 0.072 eV below T_S. In particular, the intensity of the mode at 0.065 eV nearly doubles and the peak width falls to one-half at low temperatures. According to Ref. [22], these infrared active phonons are assigned to the Co-O bond stretching modes, which are sensitive to the orbital state of Co^{3+} ion via the modulation of Co-O covalency. Specifically, the mode around 0.065 eV is assigned to the stretching mode originating from the Co site with the Jahn-Teller distortion [22]. Such phonon activation and sharpening suggest that the Jahn-Teller distortion coupled to the Co 3d orbital is strongly enhanced below T_S.

On the basis of these results, we henceforth discuss the origin of the structural phase transition. One might consider the ordering of oxygen vacancies, which would strongly modify the Co 3d-orbital state via the Co-O covalency. Indeed, the superstructure due to the ordering of oxygen vacancies is proposed in thin film of $La_{0.5}Sr_{0.5}CoO_{3-\delta}$ [23]. It is, however, reported that a typical temperature for the change in the crystal structure relevant to the oxygen vacancies is higher than 800 K in bulk $LaCoO_3$ [24]. Thus, this may not be the primary origin for the structural transition at T_S (=126 K) for the present system. Another more plausible scenario is the ordering of Co 3d orbitals as observed in various correlated electron systems. For example, some cobalt oxides of perovskite analog show an orbital ordering with a moderate transition temperature (~360 K) [25,26]. This scenario is also consistent with the observed change in the magnetic susceptibility, appreciable ψ dependence of the resonant scattering at the Co K edge, and the significant activation of the optical phonons coupled to Co 3d orbitals.

One possible model of the spin-orbital ordering is the HS/LS state ordering; the HS-state and LS-state sites alternately align in all the [100], [010], and [001] axes, forming the rocksalt type structure [Fig. 4(a)] [9,10,17]. In this

model, however, the net magnetization is estimated to be $1.7\mu_B$/Co, given that the local magnetic moment of the HS-state site is $3.4\mu_B$ [5,7]. This is much larger than the observed value ($0.7 \pm 0.2\mu_B$/Co). In addition, it also contradicts the fact that the magnetic structure is characterized by the propagation vector (1/4 −1/4 1/4) [27]. Alternatively, we propose several plausible models as follows. One plausible model is the spin and orbital ordered structure composed of the IS- and HS-state sites; the spin and orbital alignment is viewed as the stacking of the two dimensional sheets of IS- and HS-state sites in order of IS ↑ −IS ↑ −HS ↓ −IS ↑ ⋯ spin configuration with $d_{z^2-x^2} - d_{x^2-y^2} - d_{yz} - d_{x^2-y^2} \cdots$ orbital configuration along the [1 −1 1] direction. Here, we assumed that the orbital state of the IS state is described by $d_{x^2-y^2}$ electron and d_{xy} hole or the two others obtained from it by permutation of x, y, z due to a strong attractive interaction between a pair of these e_g electron and t_{2g} hole [7]. In this model, the expected net magnetization is estimated to be $0.65\mu_B$/Co, assuming that the local magnetic moment of IS state is $2\mu_B$ [4]. In addition, it also reconciles with the magnetic structure characterized by the propagation vector of (1/4 −1/4 1/4) [27]. Therefore, this model is compatible with the above results.

We have simulated the ψ dependence of the scattering intensity based on this spin and orbital configuration [solid curves in Fig. 3(b)]. For the calculation, we assumed several kinds of built-in lattice distortion due to the tilting of CoO_6 octahedra compatible with the monoclinic or rhombohedral symmetry. However, it turned out that they do not give rise to a significant impact on the simulated ψ dependence of the scattering intensity except the small phase shift in ψ. Therefore, we neglected these built-in lattice distortions for the present analysis. The simulation is in good agreement with the experimental data in both polarization geometries, supporting the validity of the present model. We note that there are other possible models including the LS, IS, or HS states with the orbital ordering aside from the aforementioned specific spin-orbital configuration. As examples, Figs. 4(c) and 4(d) show the spin-state ordering with the HS/LS ratio of 3/1 and the homogeneous IS state phase with the orbital ordering, respectively [28]. These models are also consistent with the observed net magnetization and ψ dependence of the resonant scattering. A further refinement of the plausible models needs a more elaborate analysis on the crystal structure. In any case, it is expected that the strain induced spontaneous magnetization is induced by the e_g- (and t_{2g}-) orbital ordering involving the IS-state and/or HS-state sites with the unique ferrimagnetic structure.

To summarize, we have investigated the Co-3d spin-orbital state in a thin film of perovskite $LaCoO_3$ by means of the x-ray diffraction, optical spectra, and magnetization measurements. We identified a lattice distortion characterized by the propagation vector with (1/4 −1/4 1/4) and a significant activation of infrared-active optical phonons coupled to the Co-3d orbital below 126 K. On the basis of these results as well as the azimuthal angle dependence of the superlattice reflection at the Co K edge, we propose that the ordering of the Co-3d orbital inherent to the strain induced IS-state and/or HS-state sites gives rise to the unique ferrimagnetism, leading to the strain induced magnetization in this correlated spin-state crossover material.

The authors thank T. Arima and D. Okuyama for enlightening discussions. This work was partly supported by a Grant-In-Aid for Science Research (No. 23840010, No. 24224009, No. 22740243) from the MEXT, FIRST Program by the Japan Society for the Promotion of Science (JSPS), and has been performed under the approval of the Photon Factory Program Advisory Committee (Proposals No. 2010G086 and No. 2009S2-008).

[1] Y. Tokura, Rep. Prog. Phys. **69**, 797 (2006).
[2] P. M. Raccah and J. B. Goodenough, Phys. Rev. **155**, 932 (1967).
[3] V. G. Bhide, D. S. Rajoria, G. R. Rao, and C. N. R. Rao, Phys. Rev. B **6**, 1021 (1972).
[4] M. A. Korotin, S. Yu. Ezhov, I. V. Solovyev, V. I. Anisimov, D. I. Khomskii, and G. A. Sawatzky, Phys. Rev. B **54**, 5309 (1996).
[5] S. Noguchi, S. Kawamata, K. Okuda, H. Nojiri, and M. Motokawa, Phys. Rev. B **66**, 094404 (2002).
[6] K. Knížek, Z. Jirák, J. Hejtmánek, M. Veverka, M. Maryško, G. Maris, and T. T. M. Palstra, Eur. Phys. J. B **47**, 213 (2005).
[7] A. Podlesnyak, S. Streule, J. Mesot, M. Medarde, E. Pomjakushina, K. Conder, A. Tanaka, M. W. Haverkort, and D. I. Khomskii, Phys. Rev. Lett. **97**, 247208 (2006).
[8] M. W. Haverkort *et al.*, Phys. Rev. Lett. **97**, 176405 (2006).
[9] K. Knizek, Z. Jirak, J. Hejtmanek, P. Novak, and W. Ku, Phys. Rev. B **79**, 014430 (2009).
[10] J. Kunes and V. Krapek, Phys. Rev. Lett. **106**, 256401 (2011).
[11] D. Fuchs, C. Pinta, T. Schwarz, P. Schweiss, P. Nagel, S. Schuppler, R. Schneider, M. Merz, G. Roth, and H. v. Löhneysen, Phys. Rev. B **75**, 144402 (2007).
[12] J. W. Freeland, J. X. Ma, and J. Shi, Appl. Phys. Lett. **93**, 212501 (2008).
[13] V. V. Mehta, M. Liberati, F. J. Wong, R. V. Chopdekar, E. Arenholz, and Y. Suzuki, J. Appl. Phys. **105**, 07E503 (2009).
[14] A. D. Rata, A. Herklotz, L. Schultz, and K. Dorr, Eur. Phys. J. B **76**, 215 (2010).
[15] D. P. Kozlenko, N. O. Golosova, Z. Jirák, L. S. Dubrovinsky, B. N. Savenko, M. G. Tucker, Y. Le Godec, and V. P. Glazkov, Phys. Rev. B **75**, 064422 (2007).
[16] M. M. Altarawneh *et al.*, Phys. Rev. Lett. **109**, 037201 (2012).

[17] H. Hsu, P. Blaha, and R. M. Wentzcovitch, Phys. Rev. B **85**, 140404(R) (2012).
[18] J. M. Rondinelli and N. A. Spaldin, Phys. Rev. B **79**, 054409 (2009).
[19] W. S. Choi *et al.*, Nano Lett. **12**, 4966 (2012).
[20] See Supplemental Material at http://link.aps.org/supplemental/10.1103/PhysRevLett.111.027206 for the brief description on the fundamental reflections and crystal structure of $LaCoO_3$ film.
[21] V. E. Dmitrienko, Acta Crystallogr. Sect. A **39**, 29 (1983).
[22] S. Yamaguchi, Y. Okimoto, and Y. Tokura, Phys. Rev. B **55**, R8666 (1997).
[23] J. Gazquez, W. Luo, M. P. Oxley, M. Prange, M. A. Torija, M. Sharma, C. Leighton, S. T. Pantelides, S. J. Pennycook, and M. Varela, Nano Lett. **11**, 973 (2011).
[24] P. G. Radaelli and S. W. Cheong, Phys. Rev. B **66**, 094408 (2002).
[25] S. Ishiwata, W. Kobayashi, I. Terasaki, K. Kato, and M. Takata, Phys. Rev. B **75**, 220406(R) (2007).
[26] H. Nakao, T. Murata, D. Bizen, Y. Murakami, K. Ohoyama, K. Yamada, S. Ishiwata, W. Kobayashi, and I. Terasaki, J. Phys. Soc. Jpn. **80**, 023711 (2011).
[27] Y. Yamasaki *et al.* (unpublished).
[28] The IS/LS-state ordered state with a ratio of 3/1 can be viewed as the model, in which the HS site of the model shown in Fig. 4(c) is replaced by the IS site with active $d_{y^2-z^2}$ electron and d_{yz} hole orbital.